35th Annual International Conference of the IEEE EMBS
Osaka, Japan, 3 - 7 July, 2013

# Analysis of the Rotational Center Location Method in Optical Projection Tomography*

Di Dong[1], Jin Guo[2], Yujie Yang[1], Liangliang Shi[1], Dong Peng[1], Zhenyu Liu[1], Jorge Ripoll[3] and Jie Tian[1#], *Fellow, IEEE*

*Abstract*— **In Optical Projection Tomography (OPT), if the rotational center deviates from the central line of the image and this offset is not corrected during the reconstruction, serious blurring will happen in the final 3-dimensional (3D) result. Therefore, the high-precision rotational center location method is very important for OPT. However, existing methods are inconvenient because they need active participation during the location process. Thus, the automated and fast rotational center location method is in great demand. In preliminary work, we proposed an automated rotational center location method which consisted of a high Specimen Signal Intensity (SSI) sinogram selection and a coarse-fine search. Our method had an accuracy of about 1/4 pixel. However, further robustness analysis of our method is lacking. In this paper, we have investigated its location errors on sinograms with various SSIs and analyzed whether it was effective to use high SSI sinograms for rotational center location. Moreover, we have also discussed the relationship between location errors and the starting rotational angles. The experimental results showed that our coarse-fine method was robust under different starting angles. Meanwhile, the high SSI sinogram selection scheme improved the location precision.**

## I. INTRODUCTION

OPT provides 3D high-resolution images of a small specimen (between 1mm-10mm, depending on the transparency of the specimen) [1]. OPT has two imaging modes, the transmission mode [2] and the emission mode [3]. In the transmission mode, the light absorption coefficient of the specimen is measured. While in the emission mode, the fluorescence emission signal is recorded. OPT has been applied to both *ex vivo* [4] and *in vivo* specimens [5].

In the OPT, the rotational center position is very essential for high quality 3D reconstruction. If the rotational center offset is incorrect during reconstruction, the final 3D result will be seriously blurred. The image blurring level depends on the error between the true rotational center position and the position used for the reconstruction. Therefore, it is necessary to locate the rotational center before reconstruction. There are lots of methods to locate the rotational center [6], [7], [8]. However, these methods are not convenient because they need either special structures in the specimens or active participation during the location process. In preliminary work, we have developed an automated rotational center location method (coarse-fine method [9]). The experimental results showed that the coarse-fine method had a precision of 1/4 pixel. However, we have not thoroughly evaluated the robustness of the method. In this paper, we have analyzed its location errors on sinograms with various SSIs. Moreover, we have also discussed the relationship between location errors and the starting rotational angles.

This paper is organized as follows: in Section II we present an overview of the OPT reconstruction and the coarse-fine location method. Section III includes a detailed analysis of our method. Finally, the discussion and conclusions are covered in Section IV.

## II. BASIC THEORY

### A. OPT Imaging

In transmission OPT we assume that light transmitted through the tissue under inspection follows Beer's law. Given a homogeneous light beam (see Fig. 1(a)), Beer's law is represented by

$$I_1 = I_0 e^{-\int_{r_0}^{r_1} a(r)dr} \tag{1}$$

where $a(r)$ is the absorption coefficient (or the transport coefficient in the presence of scattering) of the medium and $r$ is the distance traveled by the beam. $I_0$ and $I_1$ are the light intensities at $r_0$ and $r_1$ respectively. The purpose of OPT imaging is to obtain the absorption coefficient $a(r)$ of the sample (in the case of fluorescence, this can be approximated as negative absorption – note that in doing so we are neglecting that fluorophores emit as point sources [10]), which can be used to distinguish different tissues. Furthermore, the concept of 1D projection from 2D functions can be described as a 2D Radon transform, which has played a fundamental role in the reconstruction of X-ray Computed Tomography (CT) and now OPT. The transmission OPT geometry is shown in Fig. 1(b), where $f(x,y)$ represents the light attenuation coefficient of the specimen and $g(s,\gamma)$ represents the measurement at the detector. The OPT imaging process is a Radon transform which integrates $f(x,y)$ to

*This work was supported by the National Basic Research Program of China (973 Program) under Grant 2011CB707700, the Bill and Melinda Gates Foundation, the Instrument Developing Project of the Chinese Academy of Sciences under Grant No. YZ201164, the National Natural Science Foundation of China under Grant No. 81227901, 61231004, 81027002, 81071205, 81071129, 81101095, the Fellowship for Young International Scientists of the Chinese Academy of Sciences under Grant No. 2010Y2GA03, and the NSFC-NIH Biomedical collaborative research program under 81261120414.

[1]Di Dong, Yujie Yang, Liangliang Shi, Dong Peng, Zhenyu Liu, and Jie Tian are with Key Laboratory of Molecular Imaging and Functional Imaging, Institute of Automation, Chinese Academy of Sciences, Beijing, 100190, China.

[2]Jin Guo is with School of Automation, Harbin University of Science and Technology, Harbin 150080, China.

[3]Jorge Ripoll is with the Institute of Electronic Structure and Laser, Foundation for Research and Technology-Hellas (FORTH), 71110 Heraklion, Greece.

#corresponding author, phone: 8610-82628760; Fax: 8610-62527995; e-mail: tian@ieee.org.

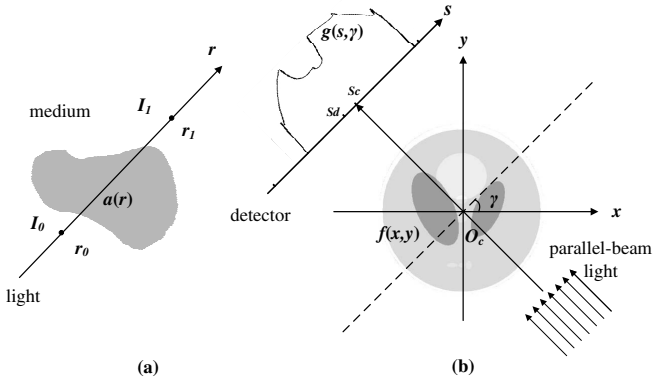


Fig. 1. Parallel-beam OPT imaging. (a) Beer's law. (b) Radon transform and parallel-beam geometry.

$g(s,\gamma)$. The OPT reconstruction is an inverse Radon transform calculating $f(x,y)$ with the known $g(s,\gamma)$.

The Filtered Back-Projection (FBP) is the most commonly used reconstruction method which is

$$f(x,y) = \frac{1}{2}\int_0^{2\pi} d\gamma \int_{-\infty}^{+\infty} |\nu| G(\nu,\gamma) e^{j2\pi\nu t} d\nu |_{t=x\cos\gamma+y\sin\gamma} \quad (2)$$

where $G(\nu,\gamma)$ is the Fourier transform of projection measurement $g(s,\gamma)$ at a fixed angle $\gamma$, and $|\nu|$ is a ramp filter applied in the Fourier domain. The FBP equation includes a double integral: the inner integral represents a ramp filtering of the projection measurement, while the outer integral represents the back-projection over all of the measurement angles. The FBP method can be effective when the scattering is low; meanwhile there are enough measurement angles. However, if the center of the rotation deviates from the center of the detector and it is not corrected before reconstruction, the FBP results will be seriously blurred. As shown in Fig. 1(b), $O_c$ is the rotational center and $s_c$ is $O_c$'s projection on the detector. $s_d$ is the center of detector. In order to avoid blurring and obtain the best possible reconstruction, the displacement between $s_d$ and $s_c$ (the rotational center position mentioned in this paper) should be found prior to reconstruction.

### B. Coarse-fine Search Method

In reference [9], we proposed a coarse-fine method to locate the rotational center automatically. The coarse-fine method includes three steps which are high SSI sinogram selection, coarse rotational center search, and fine rotational center search.

In the first step, we selected the sinograms with high SSI for the rotational center location. The SSI was defined to identify which sinograms had good quality for the rotational center search. The SSIs were calculated by using only two perpendicular projection views ($0^o$ and $90^o$). During the SSI calculation, we first segmented the specimen from the two projection views with an automated threshold. Then, the SSI of a sinogram was calculated as the sum of the specimen pixel numbers in the sinogram's corresponding rows in the two projection views. In our coarse-fine method, 10 sinograms with the highest SSI were selected for the further center location procedure.

In the second step, the center of mass method [11] was used to calculate the coarse rotational center position, known as $s_{coarse}$, for each selected sinogram. Then, we averaged all coarse positions and obtained an average position $\overline{s_{coarse}}$. This position was close to the true position but not accurate enough. Therefore, $\overline{s_{coarse}}$ was used as an initial center position in the next step.

In the final step, the variance method [6] was used to locate the rotational center. For each sinogram, we set a search region of 40 pixels around the initial position $\overline{s_{coarse}}$ with a search step of 1/8 image pixel. Then, we reconstructed this sinogram several times with all center position candidates in the search region and calculated the variance of the reconstructed images. The position with the greatest variance was the fine rotational center position known as $s_{fine}$ in this sinogram. Finally, all the $s_{fine}$ were averaged to generate the final rotational center position $\overline{s_{fine}}$.

## III. ANALYSIS

In our coarse-fine method, the sinograms used for locating the rotational center position were selected by evaluating their SSIs. It is necessary to analyze the relationship between location errors and SSIs. Besides, in our method, the starting rotational angle was $0^o$ and the SSIs were calculated using $0^o$ and $90^o$ projection views. It is important to investigate whether our method is robust with different starting rotational angles. In the following subsections, we will discuss SSI, starting rotational angle, and location error.

The following experiments were based on an *in vivo* experiment with our OPT setup (details of the OPT setup are shown in [9]). In the experiment, we acquired a fluorescence dataset on a *Drosophila melanogaster* pupa which expressed Green Fluorescent Protein (GFP). 330 projection views spanning $360^o$ were acquired with each view $500\times500$ in size. Note that, the rotational center position was tuned to 225 pixels which was 25 pixels off the detector center.

### A. The Relationship Between SSI and Location Error

We have investigated the relationship between location errors and SSIs by using the *Drosophila melanogaster* pupa dataset. We performed the coarse-fine search on all sinograms rather than only on selected sinograms, and the fine location on a sinogram using the coarse result $s_{coarse}$ on that sinogram as the initial value instead of $\overline{s_{coarse}}$. Then, we recorded both the coarse center position $s_{coarse}$ and fine center position $s_{fine}$ of each sinogram. On the other hand, we adopted $0^o$ and $90^o$ images to evaluate the SSI curve of all sinograms. Figure 2 shows the relationship between SSI and the location result, where (a) shows the coarse rotational center position, fine rotational center position and the true position of each sinogram, (b) shows the SSI of each sinogram, and (c) shows the location errors of the fine search. For the coarse search results, we see that the coarse search error of high SSI sinograms (the top 50% SSIs in the SSI curve in Fig. 2(b)) were less than 5 pixels in Fig. 2(a), which

were suitable for further fine center search. However, for the sinograms with the bottom 50% SSIs, the coarse search error could be as bad as 20 pixels (see Fig. 2(a)), due to the fact that these sinograms had no information about the specimen. In comparison, the location error while using a fine search was less than 5 pixels even on low SSI sinograms, which illustrated that the coarse-fine search method could improve the location accuracy even under conditions of very low signal to noise ratios. When considering the high SSI sinograms (the top 50% in Fig. 2(b)), the fine search had much higher accuracy yielding errors of less than 1 pixel. This is illustrated in Fig. 2(b) and Fig. 2(c), where we see that there is a direct correlation between higher SSI values and lower location errors, pointing to the fact that combining a high SSI selection prior to the rotational center search can greatly improve accuracy.

### *B. Location Results with Different Starting Rotational Angles*

We calculated the SSI using the 0° and 90° images in [9]. If the starting rotational angle changed, it was possible that the SSI values would change and the sinogram selection step could find different sinograms for the rotational center location. Therefore, it is necessary to assess the sensitivity of our method to the starting rotational angle. We also investigated the relationship between location error and the initial angle using the *Drosophila melanogaster* pupa dataset, choosing 246 projections between 0° to 270° as the initial angles, performing with each starting angle a SSI calculation, sinogram selection and center search. The results of the SSI curves, sinogram selection and location errors are shown in Fig. 3. In Fig. 3(a), we drew all 246 SSI curves in a figure which shows a significant banded structure. Note that the deviation is narrow which illustrates that SSI curves with different starting angles have a similar shape. For each SSI curve, we found the sinogram number with the highest SSI. Fig. 3(b) shows the sinogram number vs. the starting angle, where we see that the sinogram number varies from 225 to 266 having a repetition frequency of 90° which illustrates that the sinogram selection step is sensitive to the initial rotational angle. After sinogram selection, we tested the coarse-fine search on both one highest SSI sinogram and 10 highest SSI sinograms to find whether the coarse-fine search is sensitive to the initial angle. The coarse-fine search results on the highest SSI sinogram are displayed in Fig. 3(c), which shows the location error vs. the starting rotational angle yielding a maximum error of 0.2396 pixels (less than 1/4 pixel). Although the centering error was more than 1/8 pixel, it took only 0.35s to locate the center on one sinogram. In addition, we performed a coarse-fine search on 10 highest SSI sinograms (see Fig. 3(d)) where we found that the maximum error was less than 1/8 pixel. This procedure for 10 sinograms took 3.2s. In summary, the center search on one highest SSI sinogram is fast but more sensitive to the starting angle, while the center search on 10 sinograms used the average center position and was therefore less sensitive to the initial angle, albeit more time-consuming.

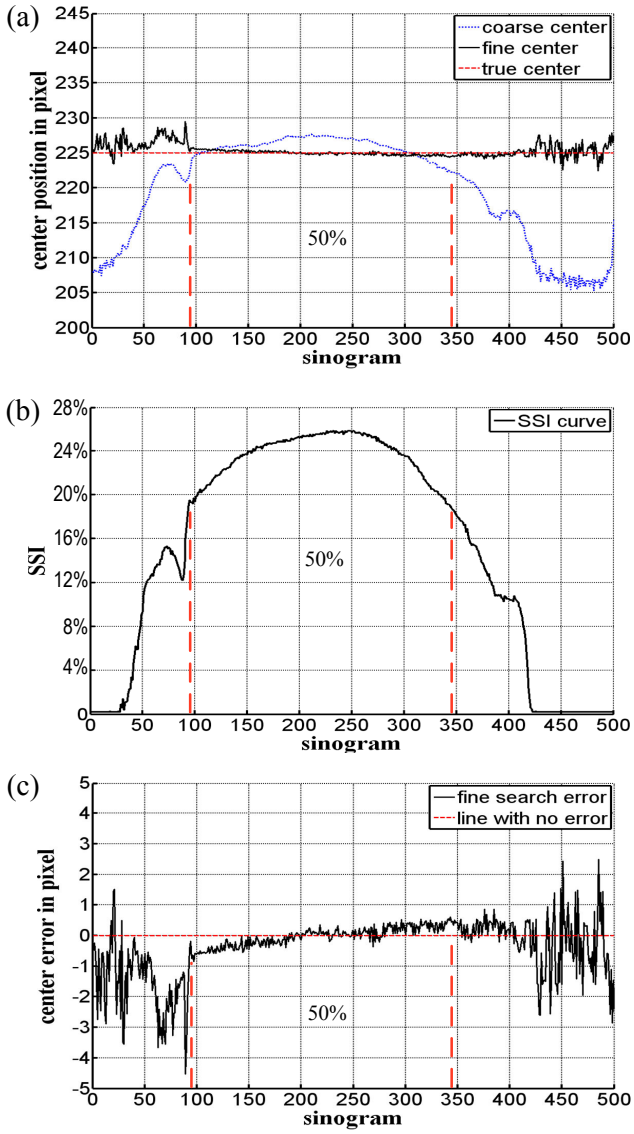


Fig. 2. Relationship between the SSI curve and the location results on the *Drosophila melanogaster* dataset. (a) Location results for each sinogram. (b) SSI curve. (c) Fine location error vs. sinogram.

## IV. CONCLUSIONS

In this paper, we have thoroughly evaluated our coarse-fine method where the SSI and the starting rotational angle were mainly considered. By performing coarse-fine centering on all sinograms, we investigated the relationship between location error and SSI. The experimental results illustrated that our coarse-fine search on a sinogram with high SSI (e.g. top 50% sinograms in SSI curve) had a high location precision (less than 1 pixel). While for the sinograms with low SSI (the bottom 50% SSIs), the location error could be 5 pixels or even larger. It can be proven that there is a direct correlation between higher SSI values and lower location errors. Therefore, the sinogram selection step can improve the accuracy of the coarse-fine method. We also performed a coarse-fine search by using various starting rotational angles

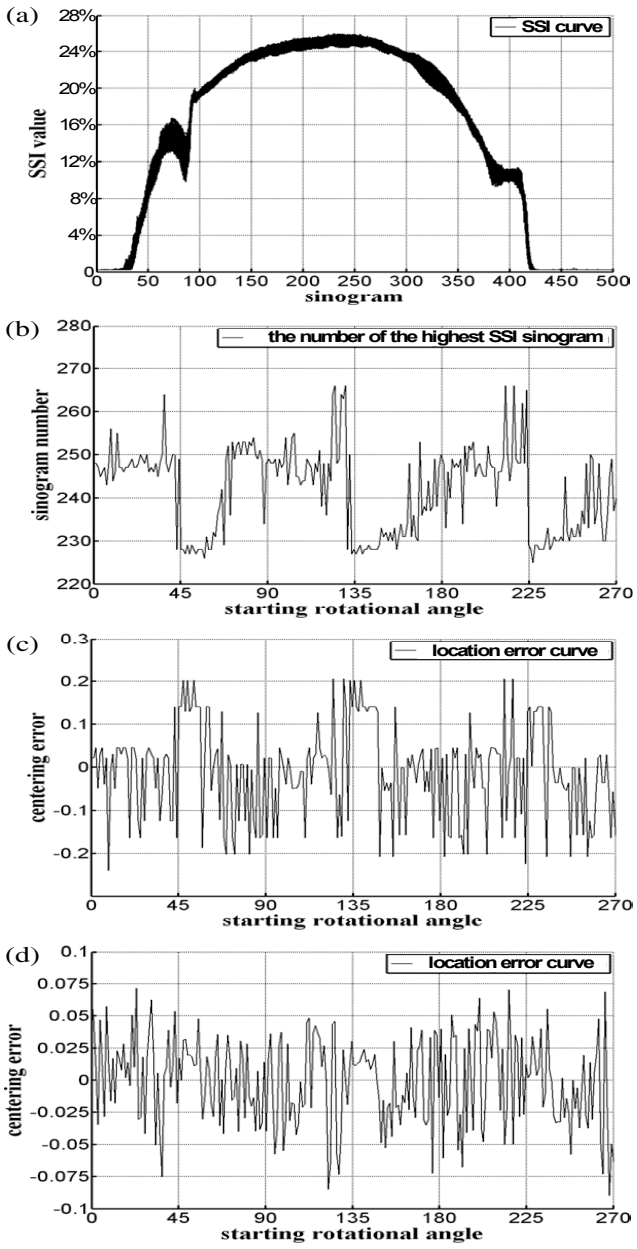


Fig. 3. Relationship between location results and starting rotational angles. (a) 246 SSI curves with different starting angles. (b) sinogram number of the highest SSI with different starting angles. (c) location error on one sinogram vs. starting angle. (d) location error on 10 sinograms vs. starting angle.

(from $0^o$ to $270^o$). Although the selected sinogram with the highest SSI was sensitive to the starting angle (it varied between 40 sinograms), the final location errors were still less than 1/4 pixel on the highest SSI sinogram. If we chose 10 highest SSI sinograms, the precision would be about 1/8 pixel.

Although the coarse-fine method showed a good robustness, there is still room for improvement. In the future, the rotational center location method with truncated data needs to be studied because truncation often happens when imaging large specimens. Besides, tilt of the rotational stage is another problem that needs to be studied, because the tiny tilt of the rotational stage is often inevitable, especially for the OPT imaging system. A possible solution for the tilt is matching the rotational center curve of all sinograms. The tilt angle of the curve will be approximately the same as the tilt angle of the rotational stage.

## REFERENCES

[1] J. Sharpe, U. Ahlgren, P. Perry, B. Hill, A. Ross, J. Hecksher-Sorensen, R. Baldock, and D. Davidson, "Optical projection tomography as a tool for 3D microscopy and gene expression studies," *Science*, vol. 296, no. 5567, pp. 541–545, 2002.

[2] F. Vasefi, E. Ng, B. Kaminska, G. H. Chapman, K. Jordan, and J. J. L. Carson, "Transmission and fluorescence angular domain optical projection tomography of turbid media." *Appl. Opt.*, vol. 48, no. 33, pp. 6448–57, Nov. 2009.

[3] C. Vinegoni, D. Razansky, J.-L. Figueiredo, M. Nahrendorf, V. Ntziachristos, and R. Weissleder, "Normalized Born ratio for fluorescence optical projection tomography." *Opt. Lett.*, vol. 34, no. 3, pp. 319–321, Feb. 2009.

[4] J. R. Walls, J. G. Sled, J. Sharpe, and R. M. Henkelman, "Resolution improvement in emission optical projection tomography." *Phys. Med. Biol.*, vol. 52, no. 10, pp. 2775–90, 2007.

[5] J. Ripoll, H. Meyer, and A. Garofalakis, "In vivo optical tomography: From diffusion to ballistic," *Opt. Mater.*, vol. 31, no. 7, pp. 1082–1085, 2009.

[6] J. R. Walls, J. G. Sled, J. Sharpe, and R. M. Henkelman, "Correction of artefacts in optical projection tomography," *Phys. Med. Biol.*, vol. 50, no. 19, p. 4645, 2005.

[7] E. Betzig, G. H. Patterson, R. Sougrat, O. W. Lindwasser, S. Olenych, J. S. Bonifacino, M. W. Davidson, J. Lippincott-Schwartz, and H. F. Hess, "Imaging intracellular fluorescent proteins at nanometer resolution," *Science*, vol. 313, no. 5793, pp. 1642–1645, 2006.

[8] U. J. Birk, M. Rieckher, N. Konstantinides, A. Darrell, A. Sarasa-Renedo, H. Meyer, N. Tavernarakis, and J. Ripoll, "Correction for specimen movement and rotation errors for in-vivo optical projection tomography," *Biomed. Opt. Express*, vol. 1, no. 1, pp. 87–96, August 2010.

[9] D. Dong, S. Zhu, C. Qin, V. Kumar, J. V. Stein, S. Oehler, C. Savakis, J. Tian, and J. Ripoll, "Automated Recovery of the Center of Rotation in Optical Projection Tomography in the Presence of Scattering," *IEEE Journal of Biomedical and Health Informatics*, vol. 17, no. 1, pp. 198–204, 2013.

[10] A. Darrell, H. Meyer, K. Marias, M. Brady, and J. Ripoll, "Weighted filtered backprojection for quantitative fluorescence optical projection tomography." *Phys. Med. Biol.*, vol. 53, no. 14, pp. 3863–3881, Jul. 2008.

[11] S. Azevedo, D. Schneberk, J. Fitch, and H. Martz, "Calculation of the rotational centers in computed tomography sinograms," *IEEE Trans. Nucl. Sci.*, vol. 37, no. 4, pp. 1525 –1540, Aug. 1990.